Materials Today Bio 15 (2022) 100282

Contents lists available at ScienceDirect

Materials Today Bio

journal homepage: www.journals.elsevier.com/materials-today-bio

Intrinsic specificity of plain ammonium citrate carbon dots for *Helicobacter pylori*: Interfacial mechanism, diagnostic translation and general revelation

Jiayue Geng [a,1], Zhuangzhuang Wang [a,1], Yanping Wu [a], Lejun Yu [a], Lili Wang [b], Quanjiang Dong [b], Chenguang Liu [a], Zhe Chi [a,c,*]

[a] College of Marine Life Sciences, Ocean University of China, No.5 Yushan Road, 266003, Qingdao, China
[b] Central Laboratory and Department of Gastroenterology, Qingdao Municipal Hospital, No.5 Donghai Middle Road, 266071, Qingdao, China
[c] Pilot National Laboratory for Marine Science and Technology, No.1 Wenhai Road, 266237, Qingdao, China

ARTICLE INFO

Keywords:
Helicobacter pylori
Ammonium citrate carbon dots
Intrinsic specificity
Mechanism
Ultrasensitive detection

ABSTRACT

The exploitation of carbon dots (CDs) is now flourishing; however, more effort is needed to overcome their lack of intrinsic specificity. Herein, instead of synthesizing novel CDs, we reinvestigated three reported CDs and discovered that plain ammonium citrate CDs (AC-CDs) exhibited surprising specificity for *Helicobacter pylori*. Notably, we showed that the interfacial mechanism behind this specificity was due to the affinity between the high abundant urea/ammonium transporters on *H. pylori* outer membrane and the surface-coordinated ammonium ions on AC-CDs. Further, we justified that ammonium sulfate-citric acid CDs also possessed *H. pylori*-specificity owing to their NH_4^+ doping. Thereby, we suggested that the incorporation of a molecule that could be actively transported by abundant membrane receptors into the precursors of CDs might serve as a basis for developing a plain CD with intrinsic specificity for *H. pylori*. Moreover, AC-CDs exhibited specificity towards live, dead, and multidrug-resistant *H. pylori* strains. Based on the specificity, we developed a microfluidics-assisted in vitro sensing approach for *H. pylori*, achieving a simplified, rapid and ultrasensitive detection with two procedures, shortened time within 45.0 min and a low actual limit of detection of 10.0 CFU mL^{-1}. This work sheds light on the design of more *H. pylori*-specific or even bacteria-specific CDs and their realistic translation into clinical practice.

1. Introduction

Carbon dots (CDs) are emerging as a class of photoluminescent zero-dimensional (0D) materials with great potential in biomedical applications, such as bio-imaging, bio-sensing, and drug delivery, owing to their bright photoluminescence, high photostability, tunable opto/chemical properties, low or non-toxicity, and environmental compatibility [1–3]. However, it has been argued that CDs lack specificity, which leads to their accumulation in various body parts [4]. Usually, functionalization of the surfaces of CDs has been dedicated to the development of modified CDs that possess high specificity [2,5,6], which can be achieved with pre-synthetic tailoring and post-synthetic modifications [7]. Examples include, but are not limited to, ethylenediamine (EDA)-CDs for labeling living stem cells [8] and nucleoli [9], L-aspartic acid-CDs for self-targeted imaging of brain cancer [10], aptamer-CDs for selective detection of cancer cells [11], along with a class of functionalized CDs for highly specific detection of bacteria, such as mannose-CDs for the detection of *Escherichia coli* [12], hydrocarbon-CDs for bacterial labeling and detection [13], and aptamer-CDs for the specific detection of *Pseudomonas aeruginosa* [14].

Notably, it has been claimed that some CDs and nanoparticles (NPs) possess intrinsic specificity for cells. For example, CDs prepared with the cancer ligands hyaluronic acid or folic acid as one of the precursors exhibited high specificities for the corresponding cells owing to the tailoring of those ligand moieties on the surfaces of the synthesized CDs [15,16]. The CDs prepared with mannose and ammonium citrate as precursors had a high specificity for *E. coli*, because mannose is a targeting ligand of this bacteria and it was covalently linked on the surface of the CDs [12]. However, it must be noted that mannose is also a targeting molecule for other bacteria, such as *Pseudomonas aeruginosa* [17], which may bring into question for the species-specificity of mannose for *E. coli*. Intriguingly, there was only one case in which silica-based NPs

* Corresponding author. College of Marine Life Sciences, Ocean University of China, No.5 Yushan Road, 266003, Qingdao, China.
E-mail address: cz1108@ouc.edu.cn (Z. Chi).
[1] These authors contribute equally.

https://doi.org/10.1016/j.mtbio.2022.100282
Received 14 March 2022; Received in revised form 29 April 2022; Accepted 6 May 2022
Available online 10 May 2022

without specific surface functionalization exhibited a high affinity for *Helicobacter pylori* [18]; however, the mechanism contributing to this affinity is unknown. Thus, validating whether the affinity is attributed to certain moieties on the surface of these silica-NPs awaits further study. Moreover, unlike CDs, these silica-NPs do not have any photoluminescence capability, making them unsuitable for the utilization of *H. pylori*-specific imaging and detection for the diagnosis of this pathogen. The use of intrinsically specific CDs would provide readily available target-selective indicators or drug carriers. Meanwhile, freedom from tedious and difficult post-functionalization could also reduce technical difficulties and costs in the translation of CDs from the lab to real-world applications [19]. These merits inspired us to seek a type of carbon dot that has intrinsic specificity for *H. pylori* cells.

The growing threat of *H. pylori* to humans calls for an accurate and effective diagnosis of *H. pylori* infection [20] and its total eradication from infected patients [18]. Nonetheless, asymptomatic analysis and upper gastrointestinal endoscopy are not practical for patients with *H. pylori* infections [21]. In clinical practice, diagnosis of *H. pylori* infection depends on the ^{13}C-urea breath test. However, this test can only be performed 4–8 weeks after the completion of drug treatment and is contraindicated in children and pregnant women because of the radiation [20,21]. Moreover, serum antibody tests and invasive endoscopy are also not suitable for children owing to low sensitivity and acceptability [22]. The diagnosis of *H. pylori* in stool samples may provide a promising solution to these problems [21,23]. However, the present stool antigen tests suffer from some false negative results occurring in the case of low bacterial abundance, and recent use of proton pump inhibitor (PPI) or antibiotics in patients [20]. Furthermore, these immunoassays are also confronted with the issue of expense and time-consuming preparation of specific antibodies for *H. pylori*. Therefore, efforts are still being made to develop a simple, instant, precise, and cost-effective method for detecting *H. pylori* infection [21]. It has been shown that *H. pylori* is able to transport urea and its metabolized ammonium via inner and outer membrane channel proteins [24–26], and that citric acid may interact with the urea channel of *H. pylori*, increasing the accessibility of urea [27]. Therefore, CDs derived from ammonium citrate, which contain the two *H. pylori* active targeting molecules simultaneously, may exhibit specificity for this bacterium. Moreover, ammonium citrate CDs (AC-CDs) are easily synthesized using only one compound and are highly photoluminescent with a bright blue fluorescence [28]. Thus, the direct use of *H. pylori*-specific AC-CDs may enable selective labeling, effective signal amplification, and a sensitive readout when used as probes for the detection of *H. pylori*. In addition, the availability of *H. pylori*-specific CDs may simplify the diagnostic procedure for stool specimens, which only requires the enrichment of bacteria from fecal samples, labeling *of H. pylori* with AC-CDs, and subsequent signal detection.

Based on this scientific premise, herein, AC-CDs were prepared and reinvestigated for their possible specificity for *H. pylori*. Moreover, because citric acid may interact with *H. pylori* as stated above and glucose is one of the carbon sources for *H. pylori*, citric acid CDs (CA-CDs) and glucose CDs (Glu-CDs) were separately synthesized to compare their binding specificity for *H. pylori*. Furthermore, the mechanism behind the possible specificity would be explained. With the *H. pylori*-specific CDs, a novel in vitro sensing method for *H. pylori* can be developed by directly using the CDs as an indicator, and an upgraded rapid and ultrasensitive detection of *H. pylori* can be expected, which will be specified in detail in this work.

2. Material and methods

2.1. Reagents, strains and fecal samples

All reagents were purchased from Merck KGaA (Germany). PBS buffer (1 ×) was purchased from Hopebio Biotech. Co., Ltd. (Qingdao, China). The bacterial strains used in this study were purchased from the American Type Culture Collection (ATCC) and the National Collection of Type Cultures (NCTC), including *Helicobacter pylori* ATCC® 700392™, *Escherichia coli* ATCC® 11775™, *Lactobacillus casei* ATCC® 393™, *Enterococcus faecalis* ATCC® 19433™, *Bifidobacterium bifidum* ATCC® 29521™, *Streptococcus gordonii* NCTC® 7865™, *Staphylococcus aureus* ATCC® 9144™, *Lactobacillus johnsonii* ATCC® 332™, *Ralstonia pickettii* NCTC® 11149™, *Shigella dysenteriae* NCTC® 4837™, *Klebsiella pneumoniae* NCTC® 13368™, *and Enterobacter cloacae* NCTC® 13464™. For the *H. pylori* ATCC® 700392™ control strains, *H. pylori* Sydney Strain 1 and clinical isolate *H. pylori* Chen (clarithromycin-, levofloxacin-, and metronidazole-resistant) were from the laboratory department of Qingdao Municipal Hospital; they were used in the hospital under their supervision. All *H. pylori* strains were cultivated on Karmali agar medium (Oxoid, UK) with *H. pylori* Selective Supplement (Dent) (Oxoid, UK) added at the concentration instructed by the manufacturer under a microaerophilic condition at 37 °C for 72 h [29]. Other control symbiotic gastric bacteria were grown on appropriate culture media, according to their culture guidelines. Stool samples were obtained from the laboratory department of Qingdao Municipal Hospital.

2.2. Preparation and characterization of carbon dots

AC-CDs were prepared using the dry heating method as described in a previous study [30] with some modifications. Ammonium citrate (2.0 g) was placed in a porcelain crucible and heated in an oven at 180.0 °C for 2.0 h to obtain a black powder. After cooling to 25 °C, the powder was dissolved in deionized water (10.0 mL), dispersed under ultrasound for 1.0 h, filtered three times using a polyether sulfone disposable filter (0.22 μm pore size), and then centrifuged at 35,000×*g* for 1.0 h to remove large particles. The resulting solution was further purified by dialyzing (Mw CO = 500–1000 Da) for 6 h followed by freeze-drying to obtain AC-CD powder. The AC-CDs were resuspended in deionized water at a suitable concentration for use. Citric acid CDs (CA-CDs) were synthesized according to a previously described dry heating method [6], glucose CDs (Glu-CDs) were prepared using a hydrothermal method [31], and ammonium sulfate-citric acid CDs (AS-CDs) were prepared using the dry heating method. Briefly, the precursors citric acid (1.0 g) and ammonium sulfate (1.0 g) were ground and mixed at a molar ratio of 1:1.5, and then subjected to dry heating at 200 °C for 3 h. The remaining operations were the same as those for the AC-CDs.

All of the prepared CDs were characterized by transmission electron microscopy (TEM; FEI Tecnai F20, FELMI ZFE, Australia), Fourier transform infrared spectrometry (NEXUS470, Thermo Scientific, USA), and X-ray photoelectron spectroscopy (K-Alpha, Thermo Scientific, USA). The average diameter was measured for 120 particles randomly selected from the TEM images. The zeta potentials were determined using a Zetasizer Nano Instrument (Nano ZS90, Malvern, UK). The UV–Vis absorption spectra were plotted using a UV/Vis spectrometer (UV-2600i, Shimadzu, Japan). Fluorescence spectra were recorded on a multimode microplate spectrophotometer (Infinite® M200 PRO; Tecan, Switzerland). The fluorescence quantum yields of the CDs were determined by comparison with those of quinine [32].

2.3. Determination of binding efficiency

To determine the BE of CDs to bacteria, freshly cultivated bacterial cells at log phase were collected by scraping from plates (for *H. pylori*) or by centrifugation at 5000×*g* for 10.0 min at 25.0 °C (for the remaining bacteria), washed twice with 1 × PBS, and resuspended in 1 × PBS (1.0 mL) to a final density of 1.0×10^7 CFU mL^{-1}. Each bacterial suspension was then incubated with a purposed CD (300.0 μg mL^{-1}) for 30.0 min with gentle shaking at 37.0 °C. The mixture was centrifuged at 6000×*g* for 5.0 min at 25.0 °C, and washed twice with 1 × PBS to remove unbound CDs. The pellet was resuspended in 1 × PBS (1.0 mL), and the fluorescence intensity of the suspension was recorded using a multi-mode microplate spectrophotometer at the excitation wavelength for each CD. Correspondingly, a suspension containing bacterial cells without

incubation with CD was used as a control to eliminate background interfering fluorescence at each excitation wavelength. To translate the fluorescence intensity of the CDs to the mass of the CDs, calibration curves were constructed between the CD concentration (***x***) (0, 10, 20, 30, 40, 50, 60, 70, 80, 90, 100 ng mL^{-1}) and the corresponding fluorescence intensity (***y***) in 1 × PBS (1.0 mL). The corresponding equations were: y = 17.2× - 6.1 ($R^2 = 0.9925$) for AC-CDs; y = 12.7x + 9.8 ($R^2 = 0.9972$) for CA-CDs; and y = 1.8x + 0.6 ($R^2 = 0.9994$) for Glu-CDs. The binding efficiency (BE) was defined as the nanograms of bacteria-bound CDs per optical density ($OD_{600\ nm}$) of bacteria.

2.4. Observation of binding with laser confocal microscopy

Bacterial cells to be tested (density of 1.0 × 10^7 CFU mL^{-1}) were incubated with AC-CDs (300.0 μg) or 3,3′-dioctadecyloxacarbocyanine perchlorate (DiO) (5.0 μg) or propidium iodide (PI) (10.0 μg) in 1 × PBS (1.0 mL) for 15.0 min. They were then centrifuged at 6000×*g* for 5.0 min at 25.0 °C, washed twice with 1 × PBS, and resuspended in 1 × PBS (1.0 mL). The suspension was observed using a laser confocal microscope (ZEISS LSM 800, Carl Zeiss, USA) at an excitation wavelength of 365 nm (for AC-CDs) or 484 nm (for DiO) or 482.0 nm (for PI). Fiji/ImageJ software was used for the analysis of colocalization and calculation of colocalization coefficient (Rr) [33] for AC-CDs or dye-stained bacterial cells.

2.5. Hierarchical treatment of the H. pylori cell wall

Layer-by-layer treatment of *H. pylori* to destroy the cell wall structure was referred to a previously described method [34] with minor modifications. Briefly, freshly cultivated *H. pylori* cells were harvested to prepare a suspension (1.0 × 10^7 CFU mL^{-1} in 1 × PBS). The suspension was then subjected to sequential treatment by first incubating with proteinase K (100.0 μg mL^{-1}) for 30.0 min with gentle shaking at 37.0 °C. After the proteinase K-treated cells were collected by centrifugation (6000×*g* for 5.0 min) and resuspended, EDTA (10.0 mM) was added and the cells were incubated for 30.0 min at 37.0 °C in 1 × PBS (1.0 mL). After this, the proteinase K and EDTA-treated *H. pylori* cells were subjected to treatment with lysozyme (2.0 mg mL^{-1}) at 37.0 °C for 2.0 h in 1 × PBS (1.0 mL) containing 20% sorbitol. After each treatment, commercial kits (MDBio, Co., Ltd., Qingdao, China) were used to determine the contents of amino acids/oligopeptides, phospholipids and reducing sugars in the supernatant. The BE between the treated cells and AC-CDs was measured as described above. Untreated *H. pylori* cells were used as the controls. Scanning electron microscopy was used to observe the morphology of the bacteria after each treatment according to previous protocols [35]. Laser confocal microscopy was used to visualize differences in AC-CD binding between untreated and proteinase K-treated *H. pylori* cells.

2.6. Competitive inhibition assay

An *H. pylori* suspension (1.0 × 10^7 CFU mL^{-1} in 1 × PBS) was prepared as described previously and citric acid (0.1 mM), ammonium citrate (0.1 mM), ammonium chloride (0.3 mM), or urea (0.15 mM) was added to the suspension, which was then incubated at 37.0 °C for 1.0 h. Subsequently, 300.0 μg mL^{-1} AC-CDs was added to each solution, which were then incubated at 37.0 °C for 1.0 h, followed by the determination of the BE of AC-CDs to *H. pylori*.

2.7. Determination of NH_4^+ content of CDs

The content NH_4^+ was tested according to previous work [36] using Nessler's reagent with the final concentration of each tested CD at 50.0 μg mL^{-1} in water. The reagent 18-crown-6 was used to scavenge NH_4^+ from the AC-CDs. First, AC-CDs (1.0 mL, 50.0 μg mL^{-1}) were mixed with the same volume of 18-crown-6 for 2.0 h under shaking at 37.0 °C; thereafter, chloroform was added to the same volume, and the reaction liquid was shaken enough to fully mix before centrifuging for 30 s at 12, 000×*g*. The lower layer of the resulting solution was extracted and subjected to high-resolution mass spectrometry (Q Exactive™ Hybrid Quadrupole-Orbitrap™ Mass Spectrometer, Thermo Scientific, USA). The 18-crown-6 treated AC-CDs in the upper layer were collected and their NH_4^+ content was measured using Nessler's assay to determine the BE to *H. pylori*. The binding was observed under laser confocal microscopy as described above.

2.8. Staining of live/dead H. pylori

Freshly cultivated (log phase) *H. pylori* was used as the live cells; dead cells were prepared by exposing the live cells on agar plates to UV light for 1.0 h. Live/dead cells were collected from the plates, washed with 1 × PBS, and resuspended in 1 × PBS to reach a final density of 1.0 × 10^7 CFU mL^{-1}. AC-CDs (200.0 μg mL^{-1}) and PI dye (5.0 μg mL^{-1}) were added to a suspension of live or dead *H. pylori* cells for staining. The BEs of AC-CDs to live and dead *H. pylori* cells were measured as previously described. Laser confocal microscopy was used to visually observe all of the stained *H. pylori* cells.

2.9. In vivo imaging assay

C57BL/6 mice were used to evaluate the in vivo imaging effects of the AC-CDs. The mice were starved for 12 h in advance to empty their stomachs. A solution containing AC-CDs (5.0 mg mL^{-1}, 0.3 mL) was administered to mice by oral gavage. After 1.0 h, the mice hair was molted and the animals were observed in an in vivo imaging apparatus (Newton 7.0, Vilber, USA). Starved untreated mice were used as controls. The animal assays were approved and supervised by the Animal Ethics Committee of the Ocean University of China. All the procedures of animal assays were conducted by trained personal and the animal suffering was minimized. After an animal assay was finished, animals were anesthetized and sacrificed. The corpses were disposed by the specific agency of the Ocean University of China.

2.10. In vitro detection of AC-CDs

The in vitro detection range and limit of detection for *H. pylori* with AC-CDs were determined according to our previous study [37] using only AC-CDs as the indicator. The preparation of simulated human stool samples and microfluidics-assisted treatment of samples are also referred to in this previous work. AC-CDs (200.0 μg mL^{-1}) were incubated with the treated samples for 20.0 min at 37.0 °C. Following low-speed centrifugation, the fluorescence intensity of the collected bacteria was measured and the data were converted to the cell density of *H. pylori* according to the calibration curve.

2.11. Statistical analysis

Statistical analysis was performed using GraphPad Prism 5 (GraphPad Software Inc., USA). Experiments were conducted in triplicate ($n = 3$), and the results are expressed as the mean ± standard deviation. Comparative studies of means were performed using a one-way analysis of variance. Statistical significance was set at $P < 0.05$.

3. Results and discussion

3.1. Purposed CDs are properly obtained

AC-CDs and CA-CDs were prepared using the dry heating method, whereas Glu-CDs were prepared using the hydrothermal method. The transmission electron microscopy (TEM) images in Fig. 1a–c revealed that the AC-CDs, CA-CDs and Glu-CDs were almost spherical in shape and well dispersed in water without aggregation; their average diameter was 2.9 ± 0.6 nm (AC-CDs), 3.8 ± 0.6 nm (CA-CDs), and 4.2 ± 0.9 nm (Glu-

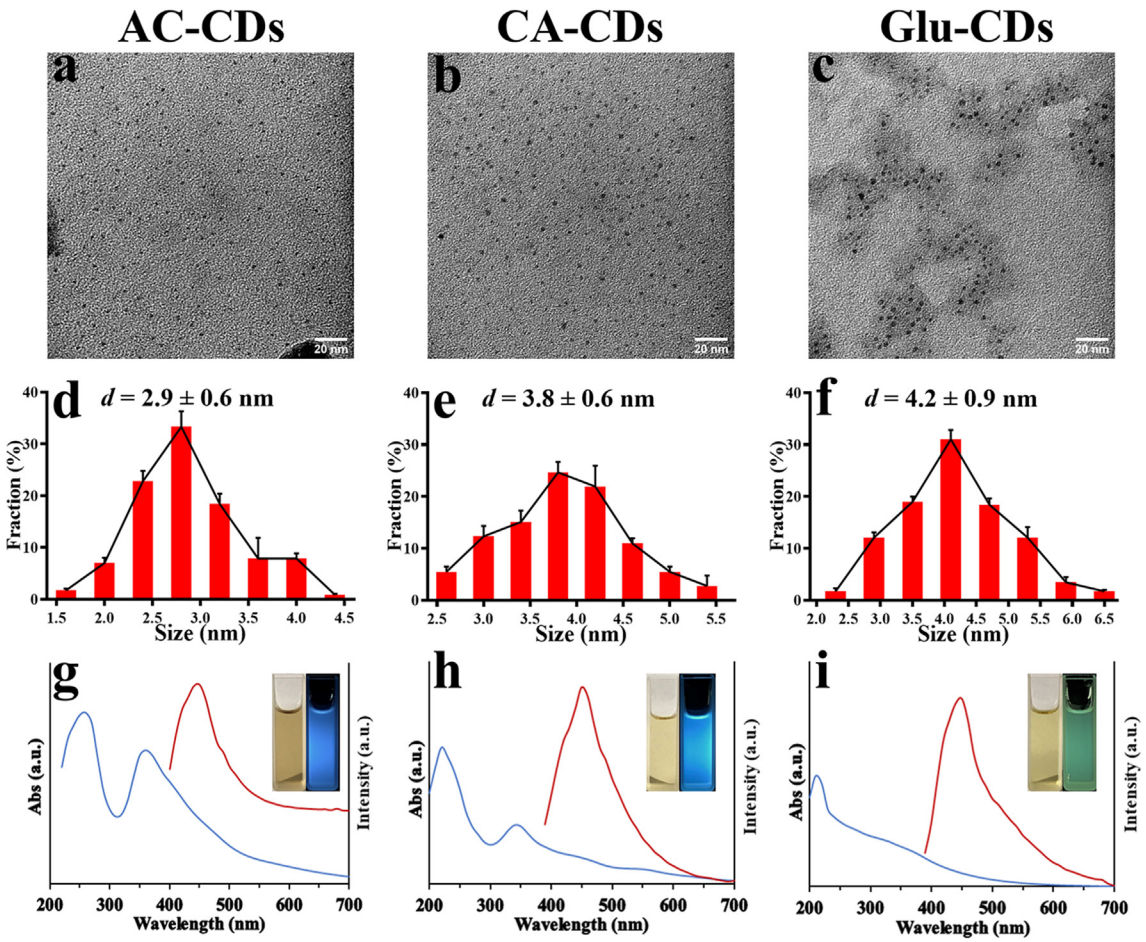

Fig. 1. Characterization of AC-CDs, CA-CDs, and Glu-CDs. (a, b, c) Transmission electron microscopy (TEM) images of the CDs. Scale bar = 20.0 nm (d, e, f) Average particle size and size distribution and of the CDs measured by TEM. Data are presented as means ± SD ($n = 3$). (g, h, i) UV–Vis absorption and fluorescence spectra of the CDs. Inset: appearances of water solutions of the CDs and their fluorescence after excitation with UV light.

CDs) (Fig. 1d–f). Aqueous solutions of the CDs emitted blue (AC-CDs and CA-CDs) or green (Glu-CDs) fluorescence when irradiated with UV light (inset in Fig. 1g–i). The UV–Vis absorption and photoluminescence (PL) spectra of the AC-CDs, CA-CDs, and Glu-CDs (Fig. 1g–i) are in close agreement with that of previous reports [30,38,39]. Moreover, the quantum yields of AC-CDs, CA-CDs, and Glu-CDs were 11.5%, 8.3%, and 1.2%, respectively, which are comparable to those previously reported [30,32,38]. These results indicate the successful synthesis of these three CDs.

Furthermore, X-ray photoelectron spectroscopy (XPS) was employed to characterize the elemental composition and surface chemical bonds of the CDs (Fig. 2). As shown in Fig. 2a, the major peaks of the AC-CDs indicate the presence of C, N, and O atoms [30,40,41]. The high-resolution spectrum of C1s for AC-CDs (Fig. 2b) was split into three components related to C–N bonds (285.2 eV), C–C bonds (284.7 eV), and C═N bonds (287.8 eV). The high-resolution O1s spectrum of AC-CDs showed two peaks at 531.2 and 532.5 eV, which were related to C═O and C–O bonds, respectively (Fig. 2c). There was one peak belonging to the major nitrogen-containing group N–H/C–N centered at 399.9 eV in the high-resolution XPS pattern of N1s (Fig. 2d), which showed that the N atom was indeed doped into the AC-CDs. The XPS survey spectra indicated that the CA-CDs possessed only C and O atoms (Fig. 2e).

The C1s peaks located at 288.9 eV and 284.9 eV (Fig. 2f) indicated the presence of C═O and C–C/C═C, respectively. The two fitted peaks at 533.7 eV and 532.1 eV in the high-resolution O1s spectrum (Fig. 2g) could be assigned to oxygen in the form of C–O and C═O bonds, respectively. Notably, CA-CDs did not contain any N atoms. Similarly, these results can be interpreted from the spectra for Glu-CDs (Fig. 2i–l). Finally, the FTIR spectra of the CDs (Fig. S1) provided supplementary information that led to the certification of N-doping in AC-CDs, as well as the presence of –OH and –COOH groups on the three CDs, and $–NH_2$ on AC-CDs, exclusively.

3.2. AC-CDs exhibit selective binding to H. pylori

To investigate the binding between CDs and bacteria, each of the three CDs was incubated with *H. pylori* 26695 (ATCC® 700392™) (see Supplementary material). After low-speed centrifugation and washing, the total weight of each type of CD bound to *H. pylori* 26695 was calculated by converting the fluorescence intensity of the bacterial cells (correlations between CD weight and corresponding fluorescence intensities are shown in the Supplementary material). The binding efficiency (BE) of each type of CD to *H. pylori* 26695 cells was evaluated by determining the weight of CDs absorbed per $OD_{600\ nm}$ of the bacterial cells. As shown in Fig. 3a, after incubation and thorough washing, the mass of AC-CDs adsorbed onto *H. pylori* 26695 cells was significantly higher than that of the other two types of CDs, with the BE values per $OD_{600\ nm}$ as 92.2 ± 1.9 ng for AC-CDs, 35.3 ± 2.2 ng for CA-CDs, and 34.2 ± 1.6 ng for Glu-CDs. The low BEs of CA-CDs and Glu-CDs might be attributed to the electrostatic interactions between CDs and cell walls or the size effect of CDs [42], which causes them to have a certain non-specificity for *H. pylori*. Nonetheless, the higher BE of AC-CDs than the other two CDs suggests that AC-CDs have greater selectivity for *H. pylori* 26695.

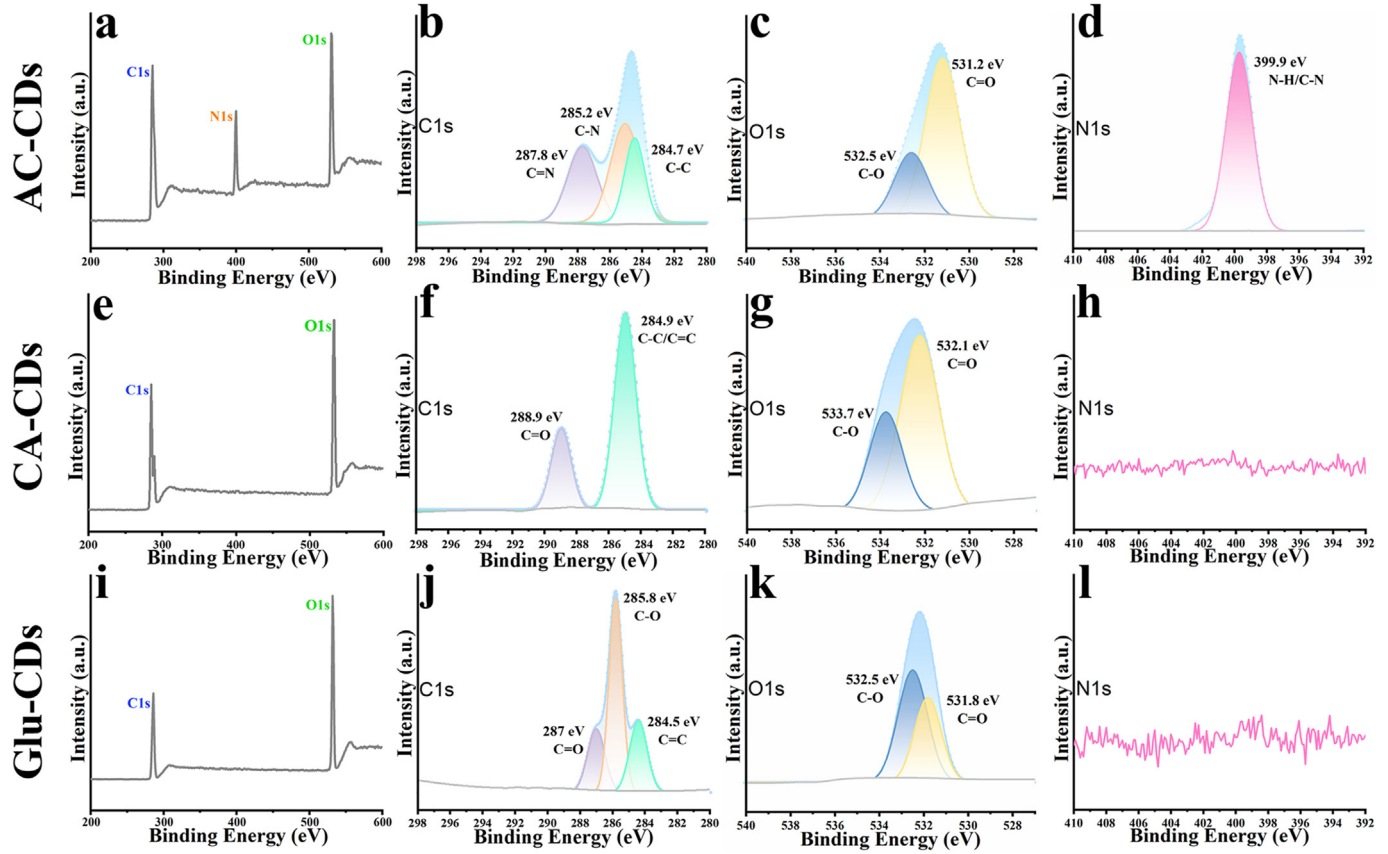

Fig. 2. X-ray photoelectron spectroscopy spectra of AC-CDs, CA-CDs, and Glu-CDs. The total spectrum and high-resolution C1s, O1s, and N1s spectra are illustrated.

Furthermore, the binding capability of AC-CDs to other *H. pylori* strains and various gastrointestinal bacteria, including *H. pylori* SS1 (Sydney strain 1), *H. pylori* Chen (a triple-resistant strain isolated from a clinical patient), *Escherichia coli*, *Streptococcus gordonii* [43], *Staphylococcus aureus* [44], *Lactobacillus johnsonii* [45], *L. casei*, *Ralstonia pickettii* [46], *Shigella dysenteriae* [47], *Enterococcus faecalis*, *Bifidobacterium bifidum* [48], *Klebsiella pneumoniae* [44], and *Enterobacter cloacae* [44], was measured. From Fig. 3b, it could be found that AC-CDs exhibited identical BEs to different *H. pylori* strains, including *H. pylori* 26695, *H. pylori* SS1, and *H. pylori* Chen [92.2 ± 1.9 ng $(OD_{600\ nm})^{-1}$, 97.8 ± 4.0 ng $(OD_{600\ nm})^{-1}$ and 90.6 ± 3.0 ng $(OD_{600\ nm})^{-1}$, respectively], whereas, the BEs of AC-CDs to other gastrointestinal bacteria were all significantly lower and below 20.0 ng $(OD_{600\ nm})^{-1}$. These very low BEs can also be ascribed to the nonspecific binding of AC-CDs to the cell surfaces of non-*H. pylori* bacteria [42].

In the following assay, *H. pylori* 26695 was used as a representative strain of *H. pylori* and laser confocal microscopy was used to further demonstrate the specificity. After incubation of AC-CDs with *H. pylori* and subsequent washing, the labeling of the bacterial cells was clearly apparent with bright blue fluorescence emitted, revealing the spiral morphology of the bacteria (Fig. 3c). This fluorescence profile matched the green fluorescence from the cells stained by 3, 3′-dioctadecyloxacarbocyanine perchlorate (DiO) (Fig. 3d and e), with a colocalization coefficient (Rr) of 0.876 (Fig. 3f). This result reflects the tight binding between AC-CDs and the cell wall of *H. pylori*. In contrast, blue fluorescence was not observed in the cell profiles of *Escherichia coli* after incubation with AC-CDs followed by washing (Fig. 3g); only green fluorescence from the DiO-stained cell membranes was observed (Fig. 3h). In addition, their merged image showed only green fluorescence (Fig. 3i), and the colocalization analysis results in a very small Rr value of 0.031 (Fig. 3j). These images indicate that AC-CDs did not bind to the cells of *E. coli*, whereas they were selective for the cell wall of *H. pylori*.

These results above indicate that AC-CDs have a higher binding capability to *H. pylori* cells, exhibiting selectivity for this bacterium.

3.3. AC-CDs mainly bind to outer membrane proteins of H. pylori

The intriguing selectivity of AC-CDs towards *H. pylori* motivated us to understand the reason for this phenomenon. First, physicochemical factors, including hydrophobicity of bacteria, particle size of the CDs, and surface charge on both the CDs and bacteria [1,30] were explored to as possible contributing factors to this specificity. However, no correlations could be found between these factors and the BEs of the three CDs with *H. pylori* (Fig. S2). Furthermore, post-modification of amine groups (Figs. S3a to 3e), which originally did not exist on CA-CDs that differed CA-CDs and AC-CDs, did not improve the binding capacity of CA-CDs to *H. pylori*; the BE of amine-modified CA-CDs (amine-CA-CDs) was 32.6 ± 5.0 ng $(OD_{600\ nm})^{-1}$ compared to 92.2 ± 1.9 ng $(OD_{600\ nm})^{-1}$ for AC-CDs (Fig. S3f). This indicated that the amine groups did not contribute to the selective binding between AC-CDs and *H. pylori*. Overall, these results suggest that there might be some unidentified functional groups on AC-CDs, and that the binding between these groups and biological molecules on the cell walls of *H. pylori*, probably membrane proteins, might contribute to the apparent selectivity above.

To examine this, the binding site for AC-CDs to *H. pylori* was first unraveled. *H. pylori* cells were treated sequentially with proteinase K, EDTA, and lysozyme [34] to digest surface proteins, decompose the outer membrane, and destroy the peptidoglycan cell wall layer-by-layer. Scanning electron microscopy (SEM) observations were performed for 4 groups *H. pylori* cells after different treatments, which were the *H. pylori* cells without any treatment, cells treated with proteinase K, cells after the EDTA treatment towards proteinase K-treated *H. pylori* cells, and cells after the lysozyme treatment towards proteinase K and EDTA

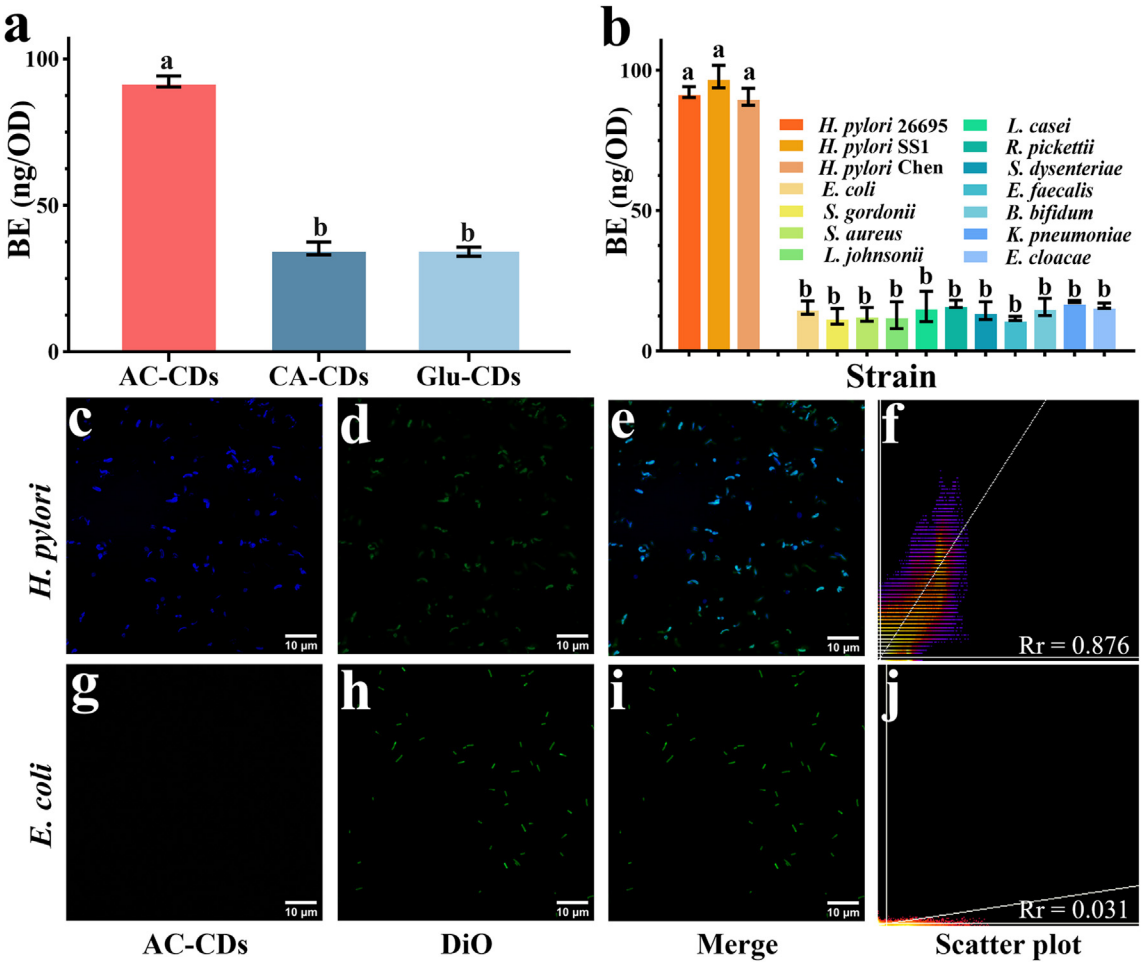

Fig. 3. Binding efficiencies (BEs) of AC-CDs, CA-CDs, and Glu-CDs to the cells of *H. pylori* 26695 strain (ATCC® 700392™) (a) and BEs of AC-CDs to various *H. pylori* strains and gastrointestinal bacteria (b). Data are presented as mean ± SD ($n = 3$); data with different lowercase letters are significantly different ($P < 0.05$). Confocal laser microscopy images of AC-CDs-binding and 3,3′-dioctadecyloxacarbocyanine perchlorate (DiO)-labeled *H. pylori* 26695 cells (c, d), their merged image (e), and the colocalization scatter plot image with colocalization coefficient (Rr) value (f). Confocal laser microscopy images of AC-CD binding and DiO-labeled *E. coli* cells (g, h), the merged image (i), and the colocalization scatter plot image with Rr value (j). For AC-CDs: excitation wavelength (λex) = 360.0 nm, emission wavelength (λem) = 465.0 nm. For DiO: λex = 484.0 nm, λem = 501.0 nm.

treated *H. pylori* cells. As shown in Fig. 4a–d, after each treatment, a higher percentage of coccoid *H. pylori* cells was found (indicated by red arrows); And almost no spiral cells were seen after treatment with lysozyme. Furthermore, chemical analysis of the resulting supernatant revealed the presence of amino acids/oligopeptides after proteinase K treatment, phospholipids after EDTA treatment, and reducing saccharides after lysozyme treatment, respectively (Fig. 4e). These results demonstrate that each treatment affected the normal morphology of *H. pylori*, which was attributed to the destruction of the structural composition of each cell wall layer.

Importantly, the determination of the BE of AC-CDs to the resulting cells after each treatment indicated that AC-CDs lost 85.1% of their binding capability after treatment with proteinase K, and another 10.0% was lost after further treatment with EDTA. However, no significant decrease in BE was observed after the third treatment with lysozyme, as compared with that of the EDTA-treated *H. pylori* cells (Fig. 4e). Moreover, laser confocal microscopy observations revealed bright fluorescence from the cell wall of untreated bacterial cells stained by either DiO or AC-CDs with positive colocalization (Rr = 0.931) (Fig. 4f–i); However, after AC-CDs were incubated with proteinase K-treated *H. pylori* cells, fluorescence from the cell wall decreased significantly in contrast to the consistently bright green fluorescence from DiO-stained cells (Rr dropped to 0.208) (Fig. 4j to m). This suggested that AC-CDs mainly bound to outer membrane proteins and, to a lesser extent, to other outer membrane components of *H. pylori*. The weak binding of AC-CDs to the peptidoglycan layers and inner membranes of the bacterium could be ascribed to non-specific binding resulting from electrostatic interactions and/or the size effect of the CDs [49].

3.4. Binding between surficial coordinated NH_4^+ on AC-CDs and outer-membrane transporters of *H. pylori* contributes to the specificity

Upon localizing the binding site for AC-CDs to *H. pylori* 26695 cells, the molecular mechanism underlying this specificity was investigated. As stated in a previous study, surficial groups play essential roles in the intrinsic or derivative functions of CDs [7]. In the above sections, it was specified that there was no positive selectivity for *H. pylori* for CA-CDs, whose precursor (citric acid) differed from that of AC-CDs (ammonium citrate) only in not having NH_4^+. This implies that the difference in surface moieties between CA-CDs and AC-CDs might contribute to their opposite selectivity for *H. pylori*. As indicated by the XPS survey (Fig. 2) and FT-IR spectra (Fig. S1), the existence of amine groups (-NH_2) is one of the different characteristics of the surficial moieties of the two CDs. However, the modification of CA-CDs with amine groups did not result in CDs with an obviously improved selectivity for *H. pylori* (Fig. S3f). In this context, characterization of the surface N-containing groups on AC-CDs was investigated.

In the higher-resolution N1s XPS spectrum of AC-CDs (Fig. S4a), a

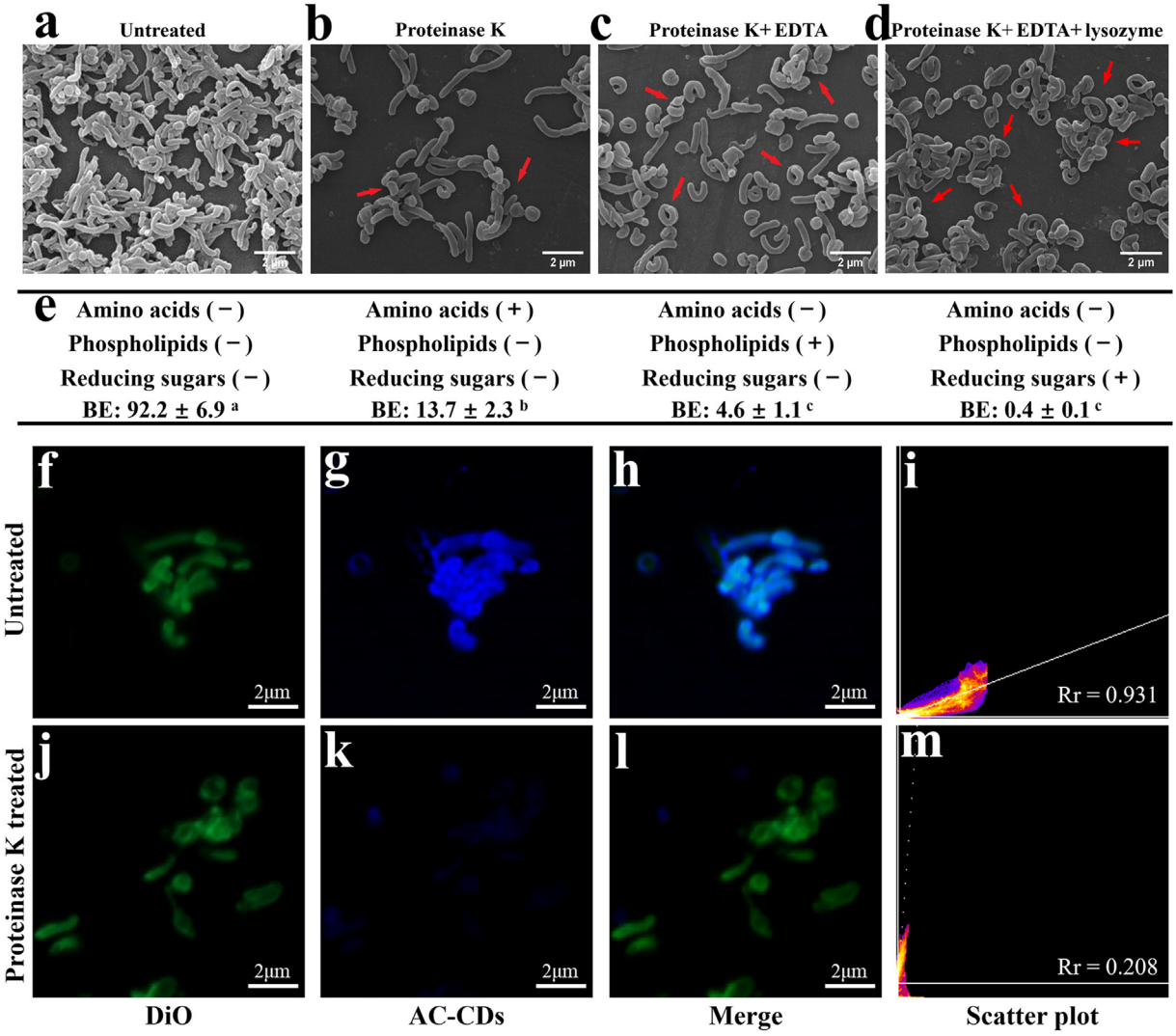

Fig. 4. Binding location of AC-CDs on the cells of *H. pylori*. (a–d) Scanning electron microscopy images of *H. pylori* cells untreated (a), after treatment with proteinase K (b), after treatment with proteinase K and then EDTA (c), and after proteinase K, EDTA, and then lysozyme treatment (d), the coccoid cells were indicated with red arrows. Chemical determination of the products and binding efficiency (BE) measured after each treatment. Data are presented as mean ± SD ($n = 3$). Data with different superscript letters are significantly different ($P < 0.05$) (e). Confocal laser microscopy images of untreated *H. pylori* cells stained by 3,3′-dioctadecyloxacarbocyanine perchlorate (DiO) and AC-CDs (f, g), their merged image (h), and the colocalization scatter plot image with colocalization coefficient (Rr) value (i). Confocal laser microscopy images of proteinase K-treated *H. pylori* cells stained by DiO and AC-CDs (j, k), their merged image (l), and the colocalization scatter plot image with colocalization coefficient (Rr) value (m). For AC-CDs: λex = 360.0 nm, λem = 465.0 nm. For DiO: λex = 484.0 nm, λem = 501.0 nm (f). (For interpretation of the references to color in this figure legend, the reader is referred to the Web version of this article.)

peak at 401.2 eV, which was assigned to the protonation state of ammonium [50–52], could be interpreted, suggesting the presence of NH_4^+ in this CDs. To verify this result, a specific test for NH_4^+ with Nessler's reagent was performed towards CDs in this work. As a result (Fig. 5a), 0.014 mg mL^{-1} NH_4^+ was measured for the AC-CD water solution, whereas the NH_4^+ content for the CA-CDs could be hardly detected. Furthermore, the strong NH_4^+ chelator 18-crown-6 [53] was used to remove NH_4^+ from the AC-CDs. Consequently, the 18-crown-6-treated AC-CDs lost almost all of their NH_4^+ content (99.0%), as determined by Nessler's assay (Fig. 5a). Further, the fraction extracted from the aqueous phase of 18-crown-6 treated AC-CDs was determined by mass spectrometry to be NH_4^+-chelating 18-crown-6 (m/z = 282.19016 [M + NH_4]$^+$) and empty 18-Crown-6 (m/z = 265.16385, [M+H]$^+$) (Figs. S4b and 4c), indicating that NH_4^+ was scavenged from the AC-CDs by 18-crown-6. More importantly, the 18-crown-6-treated AC-CDs maintained their original photoluminescence property (Fig. S5a), but completely lost their ability to bind to *H. pylori*. This was validated by a decrease in their BE to *H. pylori* from 92.2 ± 1.9 ng $(OD_{600\ nm})^{-1}$ to 33.6 ± 0.2 ng $(OD_{600\ nm})^{-1}$ (Fig. S5b), as well as laser confocal microscopy observations (Figs. S5c and d). These results demonstrate that NH_4^+ ions were indeed doped on the surfaces of AC-CDs, and more remarkably, these NH_4^+ ions contributed to the affinity binding of AC-CDs to *H. pylori*.

Notably, NH_4^+ could still be detected in the aqueous solution of AC-CDs after they were dialyzed for 6 h, lyophilized, and resuspended (see Material and Methods in SI); whereas NH_4^+ was nearly undetectable for AC-CDs after they were treated with 18-crown-6. Because of the ring structure and strong host-guest interaction via coordination bonds that recognize and bind NH_4^+ within the ring [54], 18-crown-6 has a stronger binding ability to NH_4^+ than to AC-CDs; thus, it is able to scavenge NH_4^+ from AC-CDs along with its removal from the reacting solution by organic extraction. XPS results showed that carboxyl groups were distributed on the surfaces of AC-CDs (Fig. 2); thus, these results suggest that NH_4^+ might be coordinated with carboxyl groups, which have a much weaker chelating ability than 18-crown-6, on the AC-CD surfaces. Moreover, the formation of NH_4^+-crown ethers can be attributed to the hydrogen bonds between $^+$N–H and the oxygen atoms of ether bonds in the host

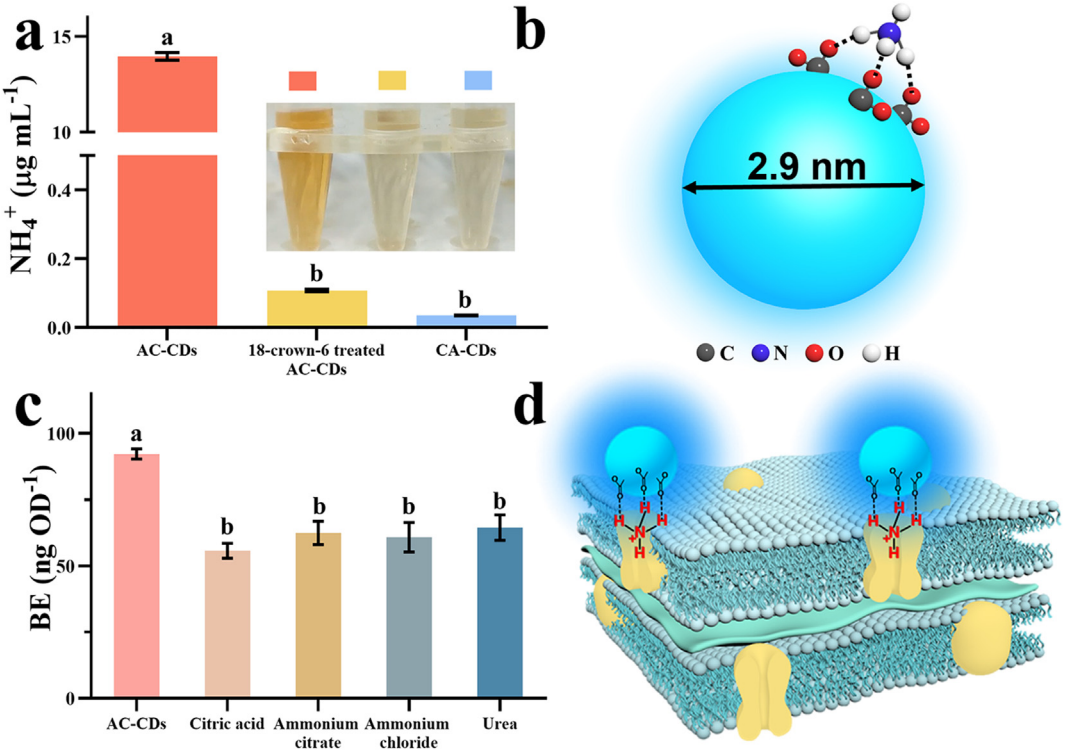

Fig. 5. (a) Determination of ammonium ion concentrations in solution from CDs as measured by Nessler's assay. Inset: Photographs of the color change after the Nessler's reagent was mixed with the aqueous CD solutions. (b) Diagram of an AC-CD with an NH_4^+ coordinated by surface carboxyl groups. (c) Binding efficiencies (BEs) of AC-CDs to *H. pylori* cells against different competitive ions. (d) 3D graphical illustration of proposed binding model between AC-CDs and *H. pylori* cell membranes. Data are presented as means ± SD ($n = 3$). Data within a graph (panels a and c) with different lowercase letters are significantly different ($P < 0.05$). (For interpretation of the references to color in this figure legend, the reader is referred to the Web version of this article.)

molecules [53]. Therefore, it was proposed that the NH_4^+ was bound to the surfaces of AC-CDs by coordinating with the oxygen atoms of carbonyls from three pendant carboxyl groups, forming a tripod arrangement via three $^+$N–H···O hydrogen bonds [53]. This might be achieved by rearrangements between the carboxyl groups and NH_4^+ powered by the energy from the dry-heating conditions of AC-CD preparation. The proposed structure of the surficial –COOH–coordinated NH_4^+ on AC-CDs is illustrated in Fig. 5b.

Previous work has shown that NH_4^+ can be excreted by *H. pylori* through urea transporters on its inner and outer membranes [24,26], indicating that these transporters have selectivity for NH_4^+. In addition, it was specified in this study that NH_4^+ doping on the surface of AC-CDs contributes to their affinity binding to the outer membrane proteins of *H. pylori*. These facts raise the question of whether the outer membrane urea transporters of *H. pylori* are the specific binding sites for NH_4^+ on AC-CDs. To answer this question, a competitive inhibition assay [12,30] using ammonium salts, citrates, and urea as competitors was implemented. Supplementation with citric acid, ammonium citrate, ammonium chloride, or urea decreased the BE of AC-CDs to *H. pylori* cells by approximately 34.0% (Fig. 5c), indicating their role as competitors in inhibiting the normal binding of AC-CDs to *H. pylori*. These results suggested that urea transporters are specific binding sites in *H. pylori* for AC-CDs. It has already been validated that outer membrane phospholipase A (OMPLA) of *H. pylori* assists in the influx of urea and NH_4^+ [26]. Thus, it is hypothesized that OMPLA is the most probable binding site for AC-CDs to *H. pylori* through the affinity of surface NH_4^+ ions on AC-CDs to this outer membrane protein, even NH_4^+ would be transported out of *H. pylori* cells after the metabolism of urea. Nevertheless, AC-CDs did not show high BEs for *S. aureus*, *K. pneumoniae*, and *E. cloacae* (Fig. 3b), although these bacteria also harbor the urease gene for the metabolism of urea to produce ammonium. As an explanation, a urease activity test showed that *H. pylori* had significantly higher urease activity than that of the other bacteria (Fig. S6). This could be ascribed to the large amount of urea synthesis in *H. pylori*, which is needed to efficiently produce ammonia/ammonium to support its thriving predominance in the acidic environment of the stomach [55]. Associated with this high yield of ammonia/ammonium, *H. pylori* is highly likely to have more abundant outer membrane urea transporters than the above-mentioned urease--positive bacteria to efficiently shuttle urea and ammonia/ammonium. Thus, this contributes to the significantly higher BE of AC-CDs to *H. pylori* over the other tested bacteria. However, further study on the ammonium transporters in *H. pylori* is still required to fully elucidate their abundance.

It is now apparent that the specific binding between surficial ammonium ions on AC-CDs and the abundant outer membrane urea transporters of *H. pylori* contributes to their selectivity over that of the other tested CDs and bacteria, thereby demonstrating the specificity of plain AC-CDs for *H. pylori* without relying on any post-modification. A plausible binding model for NH_4^+-doping AC-CDs to the cell wall of *H. pylori* is shown in Fig. 5d.

Notably, a new type of carbon dots was synthesized using citric acid and ammonium sulfate as precursors (AS-CDs); the characteristics of AS-CDs (Figs. S7 and S8) indicated they had an average particle size of 5.01 ± 0.56 nm and S atoms and NH_4^+ doped on the surfaces. Similar to that of AC-CDs (Fig. 3a and b), AS-CDs exhibited high BEs [78.3 ± 0.4 ng $(OD_{600\ nm})^{-1}$, 80.9 ± 3.3 ng $(OD_{600\ nm})^{-1}$, 77.0 ± 2.4 ng $(OD_{600\ nm})^{-1}$] to *H. pylori* 26695, *H. pylori* SS1, and *H. pylori* Chen, respectively, as well as a very low BE to the rest of the tested bacteria (Fig. S9). These results are meaningful because they demonstrate that surficial NH_4^+ doping can also be easily achieved by using another ammonium salt as a precursor to synthesize CDs in one pot. More significantly, the possession of surficial NH_4^+ renders *H. pylori*-specificity to this newly synthesized CD. Opposite to the *H. pylori*-specificity of AS-CDs, the post-modification of ethylenediamine groups on CA-CDs only changed the surface charge of amine-

CA-CDs (Fig. S3b), whereas it was unable to graft this CD any *H. pylori*-specificity (Fig. S3f), which was due to that ethylenediamine would not be actively transported by the outer membrane transporter of *H. pylori*. With these certifications, it can be proposed that the introduction of N-containing molecules, which can be actively and massively transported by membrane receptors in *H. pylori* (e.g., urea and ammonium), into the precursors of CDs, is highly likely to result in *H. pylori*-specific N-doped CDs merely by a one-pot method, without relying on secondary chemical modifications. These findings may provide a general revelation for acquiring *H. pylori*-specific CDs.

3.5. AC-CDs facilitate a simplified in vitro detection of H. pylori with ultrasensitivity

An accurate diagnosis is critical for effective treatment and eradication of *H. pylori* infection [20]. Although a series of tests are currently available for the diagnosis of *H. pylori* infection, the urea breath test is still the gold standard as a noninvasive method with common acceptance, and invasive histology is another gold standard for direct diagnosis [20]. These two tests detect live *H. pylori* based on the metabolism of urea isotopes (^{13}C- or ^{14}C-urea) and cell morphology after Giemsa staining. Other non-invasive tests for diagnosing *H. pylori* in human blood or fecal specimens with immunoassays could ignore the live or dead status of this pathogen, resulting in a higher diagnostic accuracy, but they hold obvious shortcomings including being time-consuming and expensive [56]. Notably, it has been addressed here that AC-CDs have the favorable properties of intrinsic specificity for *H. pylori*, high photoluminescence, and readily availability. Thus, AC-CDs are promising as a facile, specific, and efficient indicator in the development of a fluorescent sensor to achieve an improved and sensitive diagnosis of *H. pylori* over other current approaches.

Before developing such a sensor, the ability of AC-CDs to label live and dead *H. pylori* cells was initially investigated to evaluate the practicability of using AC-CDs to detect *H. pylori* in different states. If AC-CDs could effectively bind to both living and dead *H. pylori* cells, *H. pylori* in human feces could be detected regardless of their living status; thus, positive testing patients could be fully and correctly diagnosed. To implement this assay, newly revived and UV-light-treated fresh *H. pylori* cells were incubated with AC-CDs and then eluted. Subsequent laser confocal observation showed that the UV-treated *H. pylori* cells could be stained using propidium iodide (PI) dye, whereas the results for fresh *H. pylori* cells were negative (Fig. S10a), indicating that UV radiation [49] was lethal to *H. pylori*. Notably, AC-CDs bound to either living or dead *H. pylori* cells without significant differences, labeling the bacterial cells with bright blue fluorescence (Fig. S10a). The determination of the BE of AC-CDs towards both living [92.2 ± 1.9 ng $(OD_{600\ nm})^{-1}$] or dead (89.3 ± 2.2 ng $(OD_{600\ nm})^{-1}$] *H. pylori* cells also demonstrated that there was no significant difference between the two groups (Fig. S10b). Previously, it was demonstrated that AC-CDs were specific to *H. pylori* from a gastrointestinal bacterial community and that this specificity was identical among different strains of *H. pylori* with multiple drug resistance (Fig. 3a). Combined with these results, it can be inferred that AC-CDs specifically recognize and label *H. pylori* cells. Nevertheless, an in vivo imaging assay revealed that the fluorescence from AC-CDs could not be observed after they were administered to mice via gavage; the AC-CD fluorescence was completely blocked by a similar blue fluorescence emitted from the entire body of the tested mice (Fig. S10c). This indicated that AC-CDs can only be used as a direct fluorescence indicator for *H. pylori* in in vitro assays.

Based on these results, the use of AC-CDs for labeling and detecting *H. pylori* in vitro was investigated, and a correlation between the cell density of *H. pylori* and fluorescence intensity of bacterial cells was established. Initially, the optimal reacting conditions for the binding of AC-CDs to *H. pylori* were studied, including optimizing the concentration of AC-CDs and the incubation time with *H. pylori*. The highest fluorescence intensity was achieved when 1.0×10^7 CFU mL^{-1} *H. pylori* cells were incubated with 200.0 μg of AC-CDs (Fig. S11a) for 20.0 min (Fig. S11b) in a 1.0 mL reaction volume. These reaction conditions were consistently used for *H. pylori* cell densities lower than 1.0×10^7 CFU $m^{-1}L$ to investigate the aforementioned correlation. As illustrated in Fig. 6a, there was a linear correlation between the variation in fluorescence intensity and the *H. pylori* cell density within the range of 1.0×10^1 to 1.0×10^7 CFU mL^{-1} This correlation can be defined by equation (1): $y = 219.7\times - 16.7$, $R^2 = 0.9953$, where y represents the fluorescence intensity and x represents the log value of *H. pylori* cell density for each sample (Fig. 6b). Using this equation, the limit of detection (LOD) was calculated to be as low as 2.0 CFU mL^{-1}. This LOD is comparable to that of our previously reported biosensor (1.0 CFU mL^{-1}) [37] the easy fabrication and direct use of AC-CDs greatly simplified the sensor in this work. In addition, the LOD achieved here was much improved over that of previous studies that used an immuno-biosensor (LOD = 10^2 CFU mL^{-1}) [21] or an aptasensor (LOD = 88.0 CFU mL^{-1}) [57]. These results indicate that with AC-CDs alone, the cell density of *H. pylori* can be easily determined by reading the fluorescence signals, thereby laying a foundation for the development of a facile sensor for the detection of *H. pylori*. Notably, there was a significant difference in the fluorescence intensity values (~11.0–66.0 a.u.) between each 10-fold aliquot point of cell density within the same magnitude, e.g., 10^1–10^2, 10^3–10^4, and 10^6–10^7 (Table S1). Therefore, the use of AC-CDs as a signal amplifier can facilitate high detection resolution and sensitivity for *H. pylori*.

As conceived, AC-CDs would be applied to a non-invasive diagnosis of *H. pylori* from fecal specimens. Nonetheless, the above results were obtained under an ideal condition in clean solutions. While, it is worth noting that the matrices of actual specimens are often complicated [21] and their self-emitted fluorescence can cause severe interference when using fluorescent assays [37]. This issue was also investigated here using simulated infection-positive fecal sample prepared by artificially mixing different numbers of *H. pylori* (varying from 1.0×10^1 to 1.0×10^7 CFU mL^{-1}) with feces from healthy individuals (three 2-year-old babies and three adults) in PBS buffer (Fig. 6c, **column 2**). After the bulk solid matter was separated from the aqueous phase by low-speed centrifugation, the AC-CDs were incubated with the suspensions for 20.0 min, and then centrifuged, washed, and tested for fluorescence. An irregular fluorescence was observed regardless of the cell density of *H. pylori* in the simulated samples, validating a great influence from the fecal samples on the direct detection of *H. pylori* with AC-CDs. To address this problem, a centrifugal microfluidic plate described in our previous work [58], was applied to separate and enrich bacteria from the fecal matrices. To implement this, the simulated sample solution was loaded into the sample chamber of a microfluidic plate and subjected to horizontal centrifugation. Subsequently, ~50.0% of the *H. pylori* cells from each simulated sample were enriched in the collecting well (Fig. 6c, **column 3**), as measured by absolute quantification using real-time PCR (qPCR).

However, attention must be paid that some impurities from fecal samples, such as tiny bulk residuals, ions and proteins, may not be excluded to enter the collecting well by the microfluidic plate, thus to coexist with the enriched bacteria. These impurities may affect the binding between AC-CDs and *H pylori* as interference. To address this concerning, each microfluidics-enriched sample was reacted with AC-CDs, collected, and then the fluorescence intensity was determined. It was found these tested intensities (Fig. 6a, **column 4**) were higher than those calculated by using equation (1) (Table S2) with the corresponding qPCR determined *H. pylori* CFU (Fig. 6a, **column 3**). This result validated there still remaining some fluorescence interference on the detection of *H. pylori* with AC-CDs caused by the fecal impurities, which may come from the attachment to *H. pylori* by the fluorescence self-emitting impurities that affects the binding of AC-CDs, even the fecal samples were treated with microfluidic plates. Additionally, there still is nonspecific binding between AC-CDs and other gastrointestinal bacteria as described earlier. Because the microfluidic plate would enrich all kinds of bacteria in the simulated fecal samples, non-*H. pylori* bacteria were also able to capture some of the AC-CDs. Hence, these two factors above would both

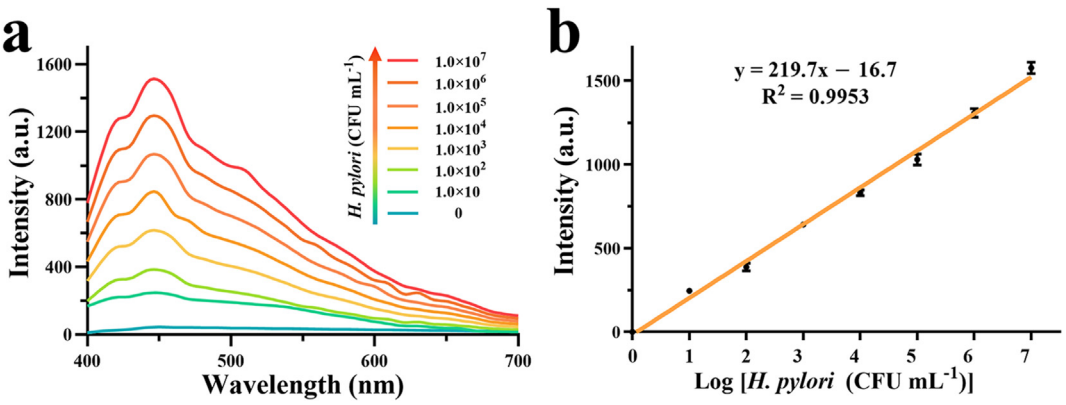

c

Items / Sample	Spiked level (CFU mL^{-1})	Microfluidics collected level (CFU mL^{-1})	Fluorescence intensity (a.u.)	Corrected level (CFU mL^{-1})	Reappearance (%)
Simulated human stool	1.0×10^7 [a]	$(5.4 \pm 0.3) \times 10^6$ [a]	1504.5 ± 3.0 [a]	$(5.4 \pm 0.2) \times 10^6$ [a]	53.4 ± 1.9 [a]
	1.0×10^6 [b]	$(5.7 \pm 0.2) \times 10^5$ [b]	1287.9 ± 3.7 [b]	$(5.1 \pm 0.1) \times 10^5$ [b]	51.3 ± 1.2 [b]
	1.0×10^5 [c]	$(5.1 \pm 0.3) \times 10^4$ [c]	1061.5 ± 2.6 [c]	$(5.1 \pm 0.2) \times 10^4$ [c]	50.7 ± 1.5 [b, c]
	1.0×10^4 [d]	$(5.6 \pm 0.1) \times 10^3$ [d]	833.0 ± 0.4 [d]	$(4.9 \pm 0.1) \times 10^3$ [d]	48.9 ± 0.4 [c, d]
	1.0×10^3 [e]	558.0 ± 2.7 [e]	612.7 ± 1.7 [e]	480.1 ± 2.7 [e]	48.0 ± 0.3 [d, e]
	1.0×10^2 [f]	59.5 ± 0.3 [f]	382.4 ± 2.4 [f]	46.2 ± 0.3 [f]	46.2 ± 0.3 [e, f]
	1.0×10^1 [g]	5.7 ± 0.1 [g]	162.9 ± 1.6 [g]	4.5 ± 0.1 [g]	45.0 ± 0.9 [f]
	0 [h]	0 [h]	44.1 ± 1.2 [h]	0 [h]	-

Fig. 6. Detection of *H. pylori* in buffer solutions and from simulated human fecal samples assisted by microfluidics. (a) Fluorescence spectra of AC-CDs from collected cells of *H. pylori* after fresh cells were incubated with AC-CDs at 1.0×10^1, 10^2, 10^3, 10^4, 10^5, 10^6, and 10^7 CFU mL^{-1}, respectively (light blue to red curves). The fluorescence spectrum of a solution containing no *H. pylori* was used as the blank control (dark blue). (b) Linear correlation between fluorescence intensities and cell densities of *H. pylori*. (c) Data for *H. pylori* detection in simulated fecal samples with AC-CDs coupled with microfluidics. Data are presented as means ± SD ($n = 3$). Data with different superscript letters are significantly different ($P < 0.05$). (For interpretation of the references to color in this figure legend, the reader is referred to the Web version of this article.)

contribute to an interfering fluorescence background that affects the accuracy of *H. pylori* detection using AC-CDs. To verify this concern, original fecal specimens without *H. pylori* were also subjected to microfluidic enrichment and AC-CDs incubation using the same procedures as described above. Consequently, an average background fluorescence intensity of 44.1 ± 1.2 a.u., was confirmed (Fig. 6a, **column 4, the bottom line**). Despite this low level of background fluorescence, it would result in a false calculation of 1.90 CFU mL^{-1} of *H. pylori* when substituted into equation (1). This would severely affect the positive/negative judgment of *H. pylori* infection when its abundance was extremely low ($<1.0 \times 10^1$ CFU mL^{-1}) in fecal specimens. Therefore, a correction for the background value was made by subtracting it from the fluorescence value of each sample. The resulting corrected detection values related to *H. pylori* density were then calculated according to equation (1) (Fig. 6c, **column 5**). The coupling of microfluidics and AC-CDs performed the recovery of *H. pylori* cell density in original fecal samples to vary from approximately 45.0–53.0% against the cell densities that ranged from 1.0×10^1 to 1.0×10^7 CFU mL^{-1} (Fig. 6c, **column 6**). Thus, the LOD obtained by combining a centrifugal microfluidic plate and AC-CDs was as low as 10.0 CFU mL^{-1}, but it did not reach the calculated limit of 2.0 CFU mL^{-1}. Nevertheless, this LOD still surpasses that of previously reported biosensors for *H. pylori*, as stated above. Thus, microfluidics and AC-CDs together contribute to the ultimate platform for the ultrasensitive detection of *H. pylori* in human feces.

In terms of time cost in using this platform, it requires 20.0 min to complete the microfluidic enrichment, another 20.0 min to incubate the suspension from the microfluidics and AC-CDs, and another 5.0 min to complete the centrifugation and washing, as described above. Altogether, one fecal specimen test for *H. pylori* can be completed in 45.0 min. This time cost has been shortened by approximately 75.0% compared to the former method using immunomagnetic beads coupled with fluorescent quantum dots [21] as well as by ~30.0% compared with that of the triple-module biosensor described in our recent study [37].

4. Conclusion

By re-investigating the biological and surfacial properties of ammonium citrate carbon dots (AC-CDs), we demonstrated that the already-synthesized plain AC-CDs have natural specificity for the whole cell of *H. pylori*, regardless of its dead, live, or multi-drug resistance status. The mechanism underlying this phenomenon is the specific binding between the abundant urea transporters in the outer membranes of *H. pylori* and surface-coordinated ammonium ions on AC-CDs. This molecular basis, together with the similar specificity of newly synthesized ammonium sulfate CDs for *H. pylori*, suggest a principle that nitrogen-containing molecules that are able to be actively and massively transported by *H. pylori* can be used as precursors to synthesize *H. pylori*-specific CDs, by proper preparation. The *H. pylori* specificity of AC-CDs, along with their characteristic luminescence, enables them to serve as an effective in vitro indicator of *H. pylori* and be used to directly label this bacterium with ease. AC-CDs coupling with a microfluidic plate for sample treatment accomplish a rapid and ultrasensitive sensing approach for *H. pylori* in fecal specimens. Remarkably, this method is simplified to have only two components and two procedures, showing its potential for further application in clinical diagnosis. The proposed principle here may also be generalized to facile preparation of other advanced CDs, such as red or near-infrared emission CDs, to possess designed bacteria-specificity without post-modification. Thereby, a broader application of specific-CDs, for example, an in vivo theragnostic for human pathogenic bacteria, can be expected.

Author statement

We claim the author contributions as follows, Jiayue Geng: Data curation, Methodology, Software. Zhuangzhuang Wang: Methodology, Visualization. Yanping Wu: Investigation, Methodology. Lejun Yu: Validation. Lili Wang: Resources. Quanjiang Dong: Resources. Chenguang Liu: Supervision. Zhe Chi: Conceptualization, Project administration, Funding acquisition, Writing - the original draft, Writing – review & editing.

Declaration of competing interest

The authors declare that they have no known competing financial interests or personal relationships that could have appeared to influence the work reported in this paper.

Acknowledgements

This work was supported by the Fundamental Research Funds for the Central Universities [Grant No. 202061010] and the Key Technology Research and Development Program of Shandong [Grant No. 2019GSF107065]. This work is also served as special gratitude and a response to the misbehavior of a research group from the "Fairy Tale" country during the planning of our collaboration that already aborted, We hope no politics shall override science.

Appendix A. Supplementary data

Supplementary data to this article can be found online at https://doi.org/10.1016/j.mtbio.2022.100282.

References

[1] X.W. Hua, Y.W. Bao, H.Y. Wang, Z. Chen, F.G. Wu, Bacteria-derived fluorescent carbon dots for microbial live/dead differentiation, Nanoscale 9 (2017) 2150–2161, https://doi.org/10.1039/c6nr06558a.
[2] P. Devi, S. Saini, K.H. Kim, The advanced role of carbon quantum dots in nanomedical applications, Biosens. Bioelectron. 141 (2019) 111158, https://doi.org/10.1016/j.bios.2019.02.059.
[3] N. Panwar, A.M. Soehartono, K.K. Chan, S. Zeng, G. Xu, J. Qu, P. Coquet, K. Yong, X. Chen, Nanocarbons for biology and medicine: sensing, imaging, and drug delivery, Chem. Rev. 119 (2019) 9559–9656, https://doi.org/10.1021/acs.chemrev.9b00099.
[4] Z. Peng, E.H. Miyanji, Y. Zhou, J. Pardo, S.D. Hettiarachchi, S. Li, P.L. Blackwelder, I. Skromne, R.M. Leblanc, Carbon dots: promising biomaterials for bone-specific imaging and drug delivery, Nanoscale 9 (2017) 17533–17543, https://doi.org/10.1039/c7nr05731h.
[5] N.C. Eemaan, P.D.K. Pierre, E.C. Yahya, C.d.T. Lisa, P. Viness, Carbon dots as nanotherapeutics for biomedical application, Curr. Pharmaceut. Des. 26 (2020) 2207–2221, https://doi.org/10.2174/1381612826666200402102308.
[6] R. Ludmerczki, S. Mura, C.M. Carbonaro, I.M. Mandity, M. Carraro, N. Senes, S. Garroni, G. Granozzi, L. Calvillo, S. Marras, L. Malfatti, P. Innocenzi, Carbon dots from citric acid and its Intermediates formed by thermal decomposition, Chemistry 25 (2019) 11963–11974, https://doi.org/10.1002/chem.201902497.
[7] F. Arcudi, L. Dordevic, M. Prato, Design, synthesis, and functionalization strategies of tailored Carbon Nanodots, Acc. Chem. Res. 52 (2019) 2070–2079, https://doi.org/10.1021/acs.accounts.9b00249.
[8] J.H. Liu, L. Cao, G.E. LeCroy, P. Wang, M.J. Meziani, Y. Dong, Y. Liu, P.G. Luo, Y.P. Sun, Carbon "quantum" dots for fluorescence labeling of cells, ACS Appl. Mater. Interfaces 7 (2015) 19439–19445, https://doi.org/10.1021/acsami.5b05665.
[9] Z.J. Zhu, Q.X. Li, P. Li, X.J. Xun, L.Y. Zheng, D.D. Ning, M. Su, Surface charge controlled nucleoli selective staining with nanoscale carbon dots, PLoS One 14 (2019), e0216230, https://doi.org/10.1371/journal.pone.0216230.
[10] M. Zheng, S.B. Ruan, S. Liu, T.T. Sun, D. Qu, H.F. Zhao, Z.G. Xie, H.L. Gao, X.B. Jing, Z.C. Sun, Self-targeting fluorescent carbon dots for diagnosis of brain cancer cells, ACS Nano 9 (2015) 11455–11461, https://doi.org/10.1021/acsnano.5b05575.
[11] H. Motaghi, M.A. Mehrgardi, P. Bouvet, Carbon dots-AS1411 aptamer nanoconjugate for ultrasensitive spectrofluorometric detection of cancer cells, Sci. Rep. 7 (2017) 10513, https://doi.org/10.1038/s41598-017-11087-2.
[12] C.I. Weng, H.T. Chang, C.H. Lin, Y.W. Shen, B. Unnikrishnan, Y.J. Li, C.C. Huang, One-step synthesis of biofunctional carbon quantum dots for bacterial labeling, Biosens. Bioelectron. 68 (2015) 1–6, https://doi.org/10.1016/j.bios.2014.12.028.
[13] S. Nandi, M. Ritenberg, R. Jelinek, Bacterial detection with amphiphilic carbon dots, Analyst 140 (2015) 4232–4237, https://doi.org/10.1039/c5an00471c.
[14] H.Y. Wang, Z. Chi, Y. Cong, Z.Z. Wang, F. Jiang, J.Y. Geng, P. Zhang, P. Ju, Q.J. Dong, C.G. Liu, Development of a fluorescence assay for highly sensitive detection of *Pseudomonas aeruginosa* based on an aptamer-carbon dots/graphene oxide system, RSC Adv. 8 (2018) 32454–32460, https://doi.org/10.1039/c8ra04819c.
[15] L.M.T. Phan, A.R. Gul, T.N. Le, M.W. Kim, S.K. Kailasa, K.T. Oh, T.J. Park, One-pot synthesis of carbon dots with intrinsic folic acid for synergistic imaging-guided photothermal therapy of prostate cancer cells, Biomater. Sci. 7 (2019) 5187–5196, https://doi.org/10.1039/c9bm01228a.
[16] H.J. Wang, J. Zhang, Y.H. Liu, T.Y. Luo, X. He, X.Q. Yu, Hyaluronic acid-based carbon dots for efficient gene delivery and cell imaging, RSC Adv. 7 (2017) 15613–15624, https://doi.org/10.1039/c7ra01417a.
[17] E. Limqueco, D. Passos Da Silva, C. Reichhardt, F.Y. Su, D. Das, J. Chen, S. Srinivasan, A. Convertine, S.J. Skerrett, M.R. Parsek, P.S. Stayton, D.M. Ratner, Mannose conjugated polymer targeting P. aeruginosa biofilms, ACS Infect. Dis. 6 (2020) 2866–2871, https://doi.org/10.1021/acsinfecdis.0c00407.
[18] D. Westmeier, G. Posselt, A. Hahlbrock, S. Bartfeld, C. Vallet, C. Abfalter, D. Docter, S.K. Knauer, S. Wessler, R.H. Stauber, Nanoparticle binding attenuates the pathobiology of gastric cancer-associated *Helicobacter pylori*, Nanoscale 10 (2018) 1453–1463, https://doi.org/10.1039/c7nr06573f.
[19] J.L. Wang, T.T. Lu, Y. Hu, X.L. Wang, Y.G. Wu, A label-free and carbon dots based fluorescent aptasensor for the detection of kanamycin in milk, Spectrochim. Acta A Mol. 226 (2020) 117651, https://doi.org/10.1016/j.saa.2019.117651.
[20] A. Tonkic, J. Vukovic, P. Vrebalov Cindro, V. Pesutic Pisac, M. Tonkic, Diagnosis of *Helicobacter pylori* infection: a short review, Wien Klin. Wochenschr. 130 (2018) 530–534, https://doi.org/10.1007/s00508-018-1356-6.
[21] L. Chen, X. Li, T. Zou, T. Wang, X. Cui, Y. Chen, C. Zhang, S. Zhao, Ultrasensitive detection of *H. pylori* in human feces based on immunomagnetic bead capture and fluorescent quantum dots, Analyst 144 (2019) 4086–4092, https://doi.org/10.1039/c9an00193j.
[22] Y.A. Leal, L.L. Flores, L.B. Garcia-Cortes, R. Cedillo-Rivera, J. Torres, Antibody-based detection tests for the diagnosis of *Helicobacter pylori* infection in children: a meta-analysis, PLoS One 3 (2008), e3751, https://doi.org/10.1371/journal.pone.0003751.
[23] Y.A. Leal, L.L. Flores, E.M. Fuentes-Panana, R. Cedillo-Rivera, J. Torres, 13C-urea breath test for the diagnosis of *Helicobacter pylori* infection in children: a systematic review and meta-analysis, Helicobacter 16 (2011) 327–337, https://doi.org/10.1111/j.1523-5378.2011.00863.x.
[24] E.F. Miller, R.J. Maier, Ammonium metabolism enzymes aid Helicobacter pylori acid resistance, J. Bacteriol. 196 (2014) 3074–3081, https://doi.org/10.1128/JB.01423-13.
[25] D.R. Scott, E.A. Marcus, Y. Wen, S. Singh, J. Feng, G. Sachs, Cytoplasmic histidine kinase (HP0244)-regulated assembly of urease with UreI, a channel for urea and its metabolites, CO_2, NH_3, and NH_4^+, is necessary for acid survival of *Helicobacter pylori*, J. Bacteriol. 192 (2010) 94–103, https://doi.org/10.1128/JB.00848-09.
[26] H.S. Vollan, T. Tannaes, D.A. Caugant, G. Vriend, G. Bukholm, Outer membrane phospholipase A's roles in *Helicobacter pylori* acid adaptation, Gut Pathog. 9 (2017) 36–48, https://doi.org/10.1186/s13099-017-0184-y.
[27] A. Shiotani, A. Saeed, Y. Yamaoka, M.S. Osato, P.D. Klein, D.Y. Graham, Citric acid-enhanced *Helicobacter pylori* urease activity in vivo is unrelated to gastric emptying, Aliment. Pharmacol. Ther. 15 (2001) 1763–1767, https://doi.org/10.1046/j.1365-2036.2001.01096.x.
[28] Z. Yang, M. Xu, Y. Liu, F. He, F. Gao, Y. Su, H. Wei, Y. Zhang, Nitrogen-doped, carbon-rich, highly photoluminescent carbon dots from ammonium citrate, Nanoscale 6 (2014) 1890–1895, https://doi.org/10.1039/c3nr05380f.
[29] Y. Cong, J. Geng, H. Wang, J. Su, M. Arif, Q. Dong, Z. Chi, C. Liu, Ureido-modified carboxymethyl chitosan-graft-stearic acid polymeric nano-micelles as a targeted delivering carrier of clarithromycin for *Helicobacter pylori*: preparation and in vitro evaluation, Int. J. Biol. Macromol. 129 (2019) 686–692, https://doi.org/10.1016/j.ijbiomac.2019.01.227.
[30] I.P.J. Lai, S.G. Harroun, S.Y. Chen, B. Unnikrishnan, Y.J. Li, C.C. Huang, Solid-state synthesis of self-functional carbon quantum dots for detection of bacteria and tumor cells, Sensor, Actuator. B Chem. 228 (2016) 465–470, https://doi.org/10.1016/j.snb.2016.01.062.
[31] N. Papaioannou, A. Marinovic, N. Yoshizawa, A.E. Goode, M. Fay, A. Khlobystoyv, M.M. Titirici, A. Sapelkin, Structure and solvents effects on the optical properties of sugar-derived carbon nanodots, Sci. Rep. 8 (2018) 6559, https://doi.org/10.1038/s41598-018-25012-8.
[32] W. Dong, S. Zhou, Y. Dong, J. Wang, X. Ge, L. Sui, The preparation of ethylenediamine-modified fluorescent carbon dots and their use in imaging of cells, Luminescence 30 (2015) 867–871, https://doi.org/https://doi.org/10.
[33] I. Del Rio-Iniguez, E. Vazquez-Chavez, C. Cuche, V. Di Bartolo, J. Bouchet, A. Alcover, HIV-1 Nef hijacks Lck and Rac1 endosomal traffic to dually modulate signaling-mediated and actin cytoskeleton-mediated T cell functions, J. Immunol. 201 (9) (2018) 2624–2640, https://doi.org/10.4049/jimmunol.1800372.1002/bio.2834.
[34] O.Y. Kim, N.T.H. Dinh, H.T. Park, S.J. Choi, K. Hong, Y.S. Gho, Bacterial protoplast-derived nanovesicles for tumor targeted delivery of chemotherapeutics, Biomaterials 113 (2017) 68–79, https://doi.org/10.1016/j.biomaterials.2016.10.037.
[35] S. Hathroubi, S. Hu, K.M. Ottemann, Genetic requirements and transcriptomics of *Helicobacter pylori* biofilm formation on abiotic and biotic surfaces, NPJ Biofilm. Microbiom. 6 (2020) 56–69, https://doi.org/10.1038/s41522-020-00167-3.
[36] Y. Zhang, Y. Wang, R. Wang, Y. Shen, J. Xu, T.J. Webster, Y. Fang, Personalized nanomedicine: a rapid, sensitive, and selective UV-vis spectrophotometry method for the quantification of nanostructured PEG-asparaginase activity in children's plasma, Int. J. Nanomed. 13 (2018) 6337–6344, https://doi.org/10.2147/IJN.S167380.

[37] Z. Wang, H. Wang, X. Cheng, J. Geng, L. Wang, Q. Dong, C. Liu, Z. Chi, Z. Chi, Aptamer-superparamagnetic nanoparticles capture coupling siderophore-Fe^{3+} scavenging actuated with carbon dots to confer an "off-on" mechanism for the ultrasensitive detection of *Helicobacter pylori*, Biosens. Bioelectron. 193 (2021) 113551, https://doi.org/10.1016/j.bios.2021.113551.

[38] Y. Dong, J. Shao, C. Chen, H. Li, R. Wang, Y. Chi, X. Lin, G. Chen, Blue luminescent graphene quantum dots and graphene oxide prepared by tuning the carbonization degree of citric acid, Carbon 50 (2012) 4738–4743, https://doi.org/10.1016/j.carbon.2012.06.002.

[39] N. Papaioannou, M.-M. Titirici, A. Sapelkin, Investigating the effect of reaction time on carbon dot formation, structure, and optical properties, ACS Omega 4 (2019) 21658–21665, https://doi.org/10.1021/acsomega.9b01798.

[40] A. Yadegari, J. Khezri, S. Esfandiari, H. Mandavi, A.A. Karkhane, R. Rahighi, R. Heidarimoghadam, L. Tayebi, E. Hashemi, A. Farmany, Bottom-up synthesis of nitrogen and oxygen co-decorated carbon quantum dots with enhanced DNA plasmid expression, Colloids Surf., B 184 (2019) 110543, https://doi.org/10.1016/j.colsurfb.2019.110543.

[41] N. Díez, A. Śliwak, S. Gryglewicz, B. Grzyb, G. Gryglewicz, Enhanced reduction of graphene oxide by high-pressure hydrothermal treatment, RSC Adv. 5 (2015) 81831–81837, https://doi.org/10.1039/C5RA14461B.

[42] B. Sun, F. Wu, Q. Zhang, X. Chu, Z. Wang, X. Huang, J. Li, C. Yao, N. Zhou, J. Shen, Insight into the effect of particle size distribution differences on the antibacterial activity of carbon dots, J. Colloid Interface Sci. 584 (2021) 505–519, https://doi.org/10.1016/j.jcis.2020.10.015.

[43] A.R. Badireddy, R. Hernandez-Delgadillo, R.I. Sanchez-Najera, S. Chellam, C. Cabral-Romero, Synthesis and characterization of lipophilic bismuth dimercaptopropanol nanoparticles and their effects on oral microorganisms growth and biofilm formation, J. Nanopart. Res. 16 (2014) 2456–2467, https://doi.org/10.1007/s11051-014-2456-5.

[44] T. Osaki, K. Mabe, T. Hanawa, S. Kamiya, Urease-positive bacteria in the stomach induce a false-positive reaction in a urea breath test for diagnosis of Helicobacter pylori infection, J. Med. Microbiol. 57 (2008) 814–819, https://doi.org/10.1099/jmm.0.47768-0.

[45] P.S. Hsieh, Y.C. Tsai, Y.C. Chen, S.F. Teh, C.M. Ou, V.A. King, Eradication of *Helicobacter pylori* infection by the probiotic strains Lactobacillus johnsonii MH-68 and L. salivarius ssp. salicinius AP-32, Helicobacter 17 (2012) 466–477, https://doi.org/10.1111/j.1523-5378.2012.00992.x.

[46] S.D. Udayappan, P. Kovatcheva-Datchary, G.J. Bakker, S.R. Havik, H. Herrema, P.D. Cani, K.E. Bouter, C. Belzer, J.J. Witjes, A. Vrieze, N. ve Sonnaville, A. Chaplin, D.H. van Raalte, S. Aalvink, G.M. Dallinga-Thie, H.G.H.J. Heilig, G. Bergström, S. van der Meij, B.A. van Wagensveld, J.B.L. Hoekstra, F. Holleman, E.S.G. Stroes, A.K. Groen, F. Bäckhed, W.M. de Vos, M. Nieuwdorp, Intestinal *Ralstonia pickettii* augments glucose intolerance in obesity, PLoS One 12 (2017), e0181693, https://doi.org/10.1371/journal.pone.0181693.

[47] A. Singh, T.G. Barnard, Adaptations in the physiological heterogeneity and viability of *Shigella dysenteriae*, Shigella flexneri and *Salmonella typhimurium*, after exposure to simulated gastric acid fluid, Microb. Pathog. 113 (2017) 378–384, https://doi.org/10.1016/j.micpath.2017.11.014.

[48] M.J. Kim, S. Ku, S.Y. Kim, H.H. Lee, H. Jin, S. Kang, R. Li, T.V. Johnston, M.S. Park, G.E. Ji, Safety evaluations of *Bifidobacterium bifidum* BGN4 and *Bifidobacterium longum* BORI, Int. J. Mol. Sci. 19 (2018) 1422–1443, https://doi.org/10.3390/ijms19051422.

[49] J. Cama, M. Voliotis, J. Metz, A. Smith, J. Iannucci, U.F. Keyser, K. Tsaneva-Atanasova, S. Pagliara, Single-cell microfluidics facilitates the rapid quantification of antibiotic accumulation in Gram-negative bacteria, Lab Chip 20 (2020) 2765–2775, https://doi.org/10.1039/d0lc00242a.

[50] G. Liu, C. Tao, M. Zhang, X. Gu, F. Meng, X. Zhang, Y. Chen, S. Ruan, Effects of surface self-assembled NH_4^+ on the performance of TiO2-based ultraviolet photodetectors, J. Alloys Compd. 601 (2014) 104–107, https://doi.org/10.1016/j.jallcom.2014.02.150.

[51] D. Yu, Z. Wei, X. Zhang, Y. Zeng, C. Wang, G. Chen, Z. Shen, F. Du, Boosting Zn^{2+} and NH_4^+ storage in aqueous media via in-situ electrochemical induced VS2/VOx heterostructures, Adv. Funct. Mater. 31 (2021) 2008743, https://doi.org/10.1002/adfm.202008743.

[52] A. Saravanan, M. Maruthapandi, P. Das, S. Ganguly, S. Margel, J.H.T. Luong, A. Gedanken, Applications of N-doped carbon dots as antimicrobial agents, antibiotic carriers, and selective fluorescent probes for nitro explosives, ACS Appl. Bio Mater. 3 (2020) 8023–8031, https://doi.org/10.1021/acsabm.0c01104.

[53] V. Rüdiger, H.-J. Schneider, V.P. Solov'ev, V.P. Kazachenko, O.A. Raevsky, Crown ether–ammonium complexes: binding mechanisms and solvent effects, Eur. J. Org Chem. 1999 (1999) 1847–1856, https://doi.org/10.1002/(SICI)1099-0690(199908)1999:8<1847::AID-EJOC1847>3.0.CO;2-Q.

[54] A. Spath, B. Konig, Molecular recognition of organic ammonium ions in solution using synthetic receptors, Beilstein J. Org. Chem. 6 (2010) 132–142, https://doi.org/10.3762/bjoc.6.32.

[55] J.W. Fahey, K.K. Stephenson, K.L. Wade, P. Talalay, Urease from *Helicobacter pylori* is inactivated by sulforaphane and other isothiocyanates, Biochem. Biophys. Res. Commun. 435 (2013) 1–7, https://doi.org/10.1016/j.bbrc.2013.03.126.

[56] G. Godbole, F. Megraud, E. Bessede, Review: diagnosis of *Helicobacter pylori* infection, Helicobacter 25 (2020), e12735, https://doi.org/10.1111/hel.12735.

[57] H. Wu, L. Gu, X. Ma, X. Tian, S. Fan, M. Qin, J. Lu, M. Lyu, S. Wang, Rapid Detection of *Helicobacter pylori* by the naked eye using DNA aptamers, ACS Omega 6 (2021) 3771–3779, https://doi.org/10.1021/acsomega.0c05374.

[58] O. Strohmeier, M. Keller, F. Schwemmer, S. Zehnle, D. Mark, F. von Stetten, R. Zengerle, N. Paust, Centrifugal microfluidic platforms: advanced unit operations and applications, Chem. Soc. Rev. 44 (2015) 6187–6229, https://doi.org/10.1039/c4cs00371c.